**Supporting Information**

# A Binder Free Facile Synthetic Approach for Amorphous, Hydrous Nickel Copper Phosphate Thin Film Electrode Preparation and its Application as Highly Stable Cathode for Hybrid Asymmetric Supercapacitors

Sachin S. Pujari[a], Sujit A. Kadam[b], Yuan-Ron Ma[b], Satish B. Jadhav[a], Sambhaji S. Kumbhar[a], Shraddha B. Bhosale[a], Vinod V. Patil[a,c], Jayavant L. Gunjakar[a], Chandrakant D. Lokhande[a], Umakant M. Patil[a]*

[a]Centre for Interdisciplinary Research, D. Y. Patil Education Society, Kasaba Bawada, Kolhapur- 416 006 (India).

[b]Department of Physics, National Dong Hwa University, Hualien- 97401 (Taiwan).

[c]School of Chemical Sciences, Punyashlok Ahilyadevi Holkar Solapur University, Solapur 413255, India.

**Supporting material for calculations:**

**For three electrode system:**

The specific capacity (C $g^{-1}$) and specific capacitance (F $g^{-1}$) was estimated from the GCD analysis as follows,

$$Q = \frac{I \times \Delta t}{w} \qquad (C\ g^{-1}) \qquad (1)$$

$$C_s = \frac{I \times \Delta t}{w \times \Delta V} \qquad (F\ g^{-1}) \qquad (2)$$

Where, w, Δt, I, and ΔV denote the mass of electroactive substance (g), discharge time (s), applied current (A $g^{-1}$), and potential window (V).

**For two electrode system:**

The charges between the cathode and anode can be balanced for excellent electrochemical results of hybrid device by using the theory of mass balance as per following equation,

$$\frac{m_+}{m_-} = \frac{C_- \times \Delta V_-}{C_+ \times \Delta V_+} \quad (3)$$

Where, $m_{(+\ or\ -)}$, $\Delta V_{(+\ or\ -)}$, and $C_{(+\ or\ -)}$ are the mass of active material (g), potential window (V), and specific capacitance (F $g^{-1}$) of positive and negative electrode, respectively. The two electrode system was used to study device performance, and its energy (E) and power density (P) calculated using following equations respectively,

$$E = \frac{0.5 \times C_s \times (\Delta V)^2}{3.6} \quad \text{(Wh } kg^{-1}\text{)} \quad (4)$$

And

$$P = \frac{E \times 3.6}{\Delta t} \quad \text{(kW } kg^{-1}\text{)} \quad (5)$$

Where, $C_s$, $\Delta V$, and $\Delta t$ represents specific capacitance, potential window and discharging time of device, respectively.

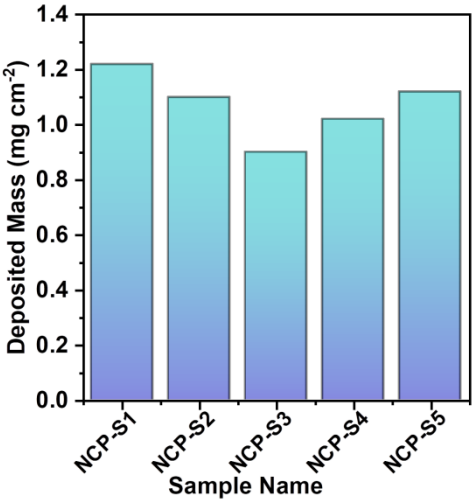


**S1:** Deposited mass of nickel copper phosphate thin film for different compositions (NCP-S1 to NCP-S5).

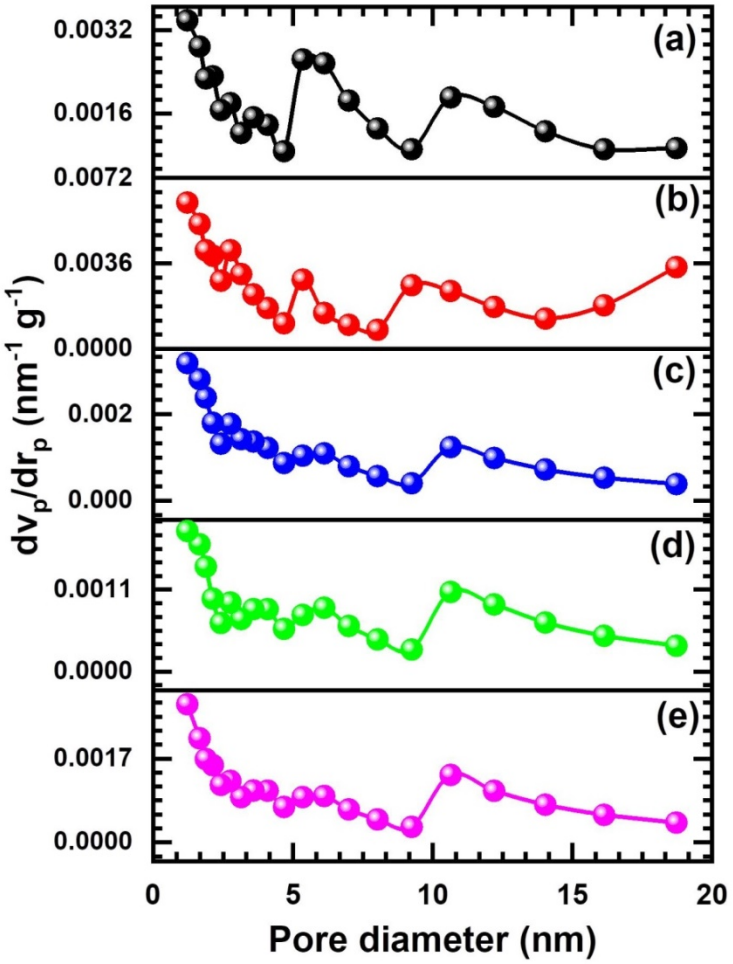


**S2:** Pore size distribution curves of samples (a) NCP-S1, (b) NCP-S2, (c) NCP-S3, (d) NCP-S4 and (e) NCP-S5.

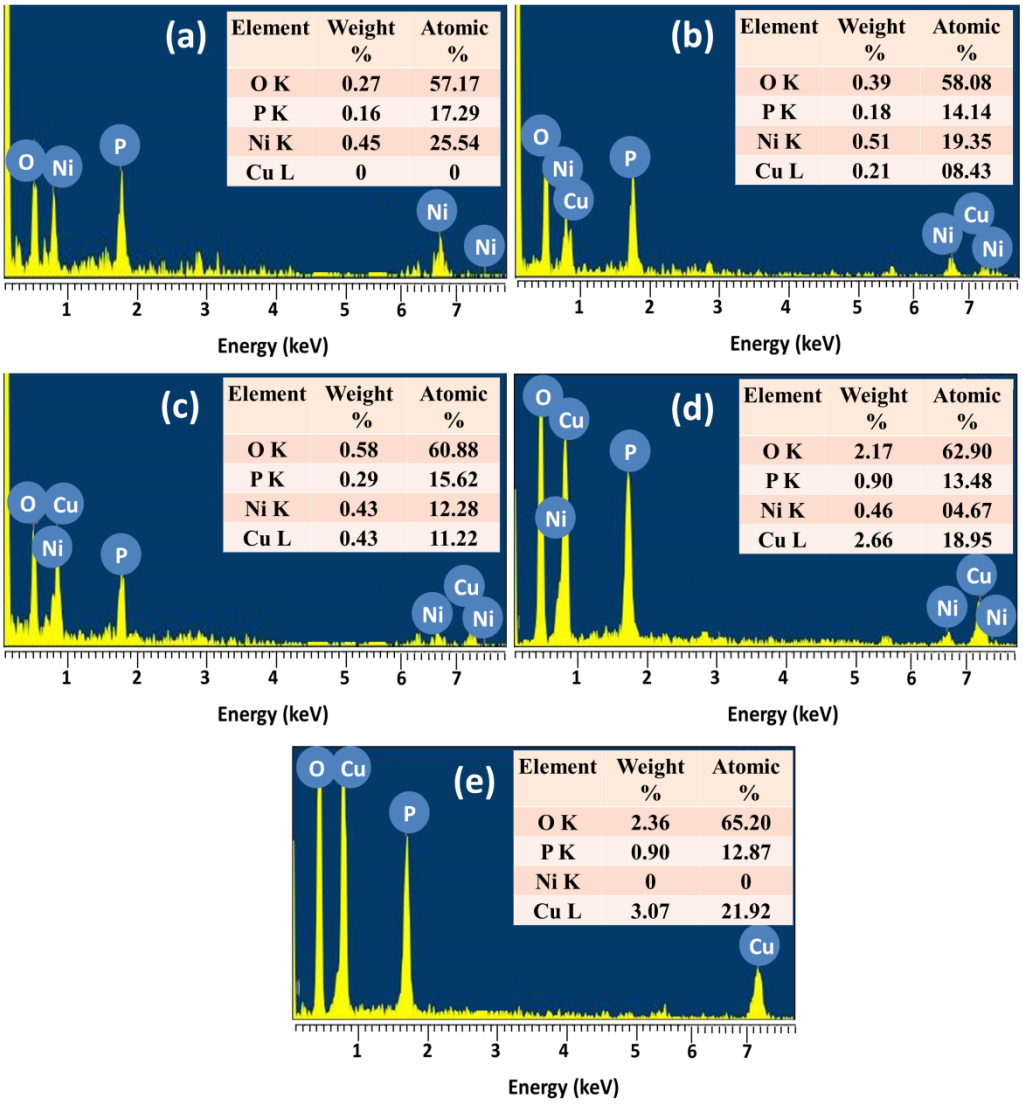


**S3:** EDS spectra of nickel copper phosphate electrodes: (a) NCP-S1, (b) NCP-S2, (c) NCP-S3, (d) NCP-S4 and (e) NCP-S5.

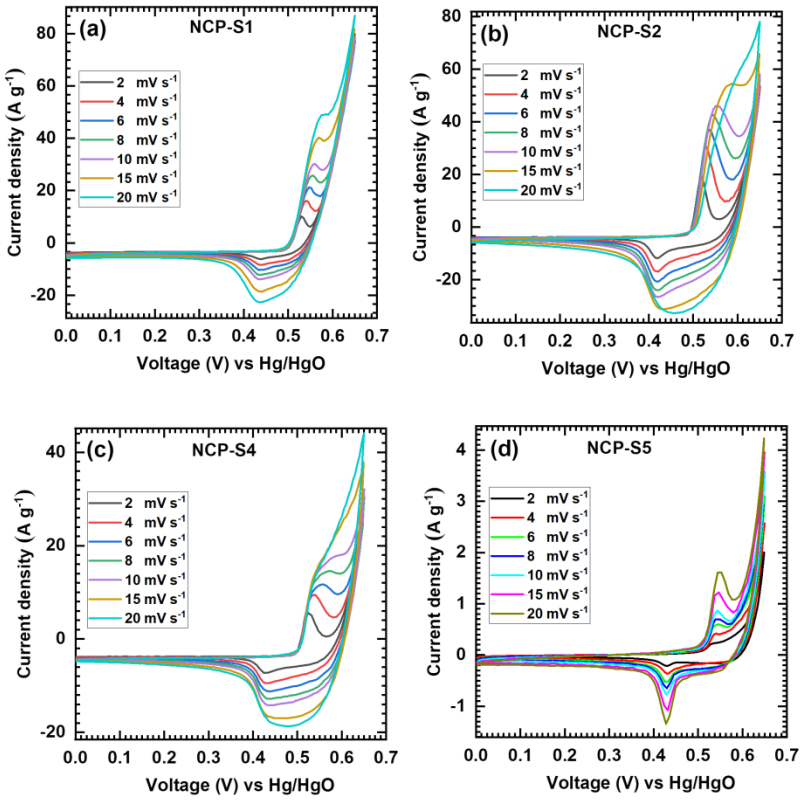


**S4:** The CV curves at different scan rates from 2-20 mV $s^{-1}$ for (a) NCP-S1, (b) NCP-S2, (c) NCP-S4, (d) NCP-S5 electrodes.

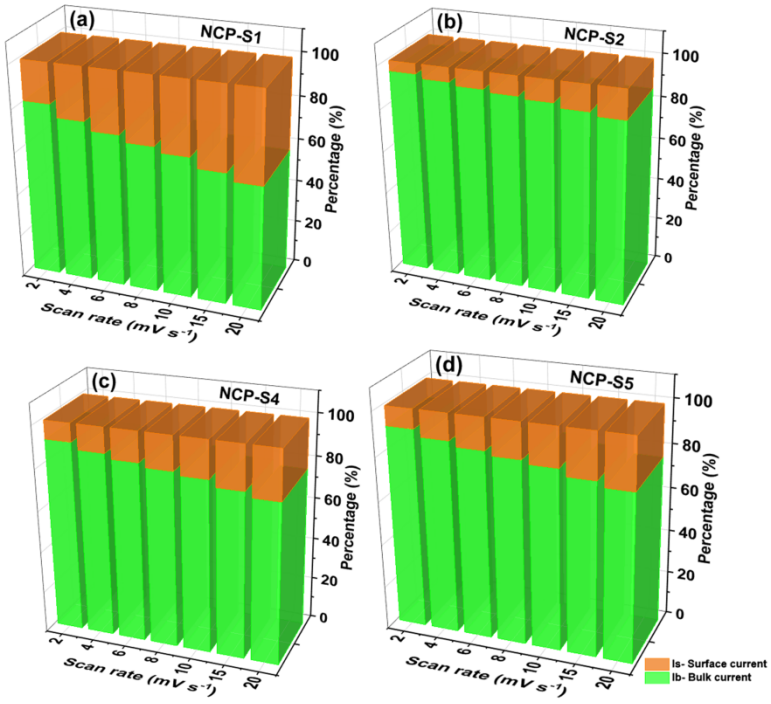


**S5:** Graphs of calculated contribution of pseudocapacitive (surface current) and battery type (bulk current) in current density at various scan rates (2 to 20 mV $s^{-1}$) (a) NCP-S1, (b) NCP-S2, (c) NCP-S4, (d) NCP-S5 electrodes.

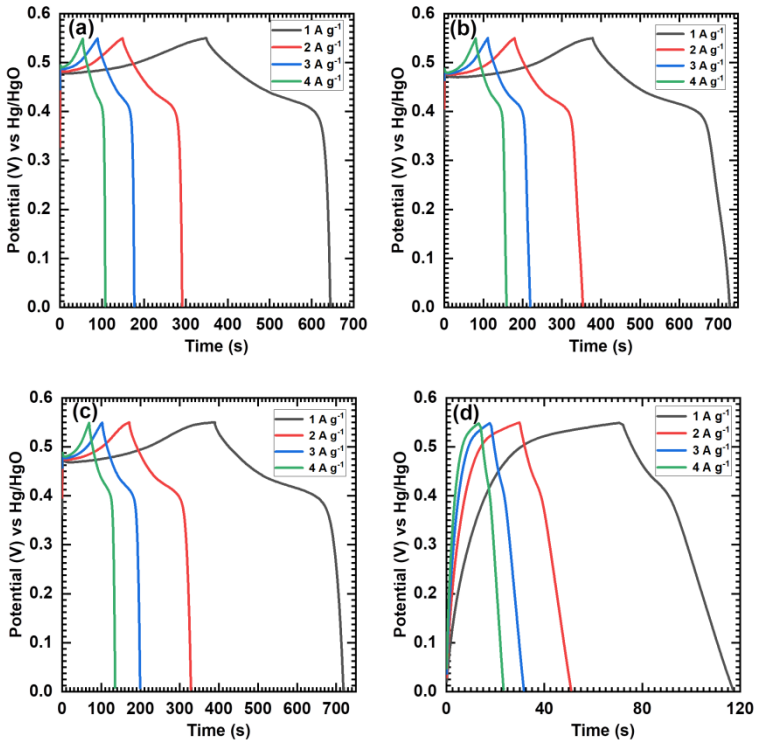


**S6:** The GCD curves at various current densities from 1-4 A $g^{-1}$ of (a) NCP-S1, (b) NCP-S2, (c) NCP-S4, (d) NCP-S5 electrodes.

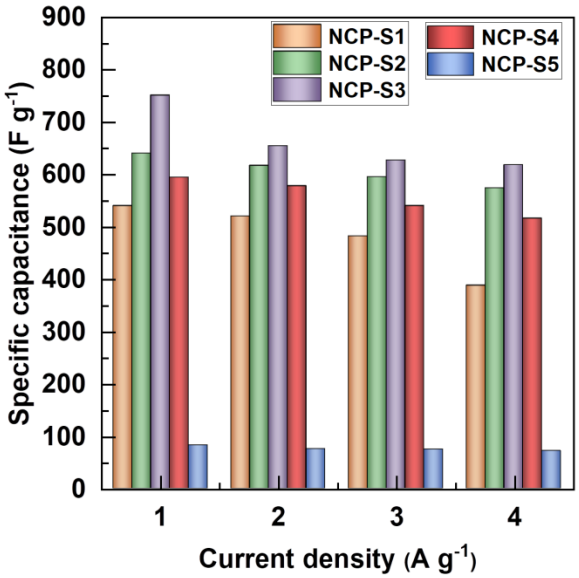


**S7:** Specific capacitance of NCP-S series thin film electrodes at various current densities (1-4 A $g^{-1}$).

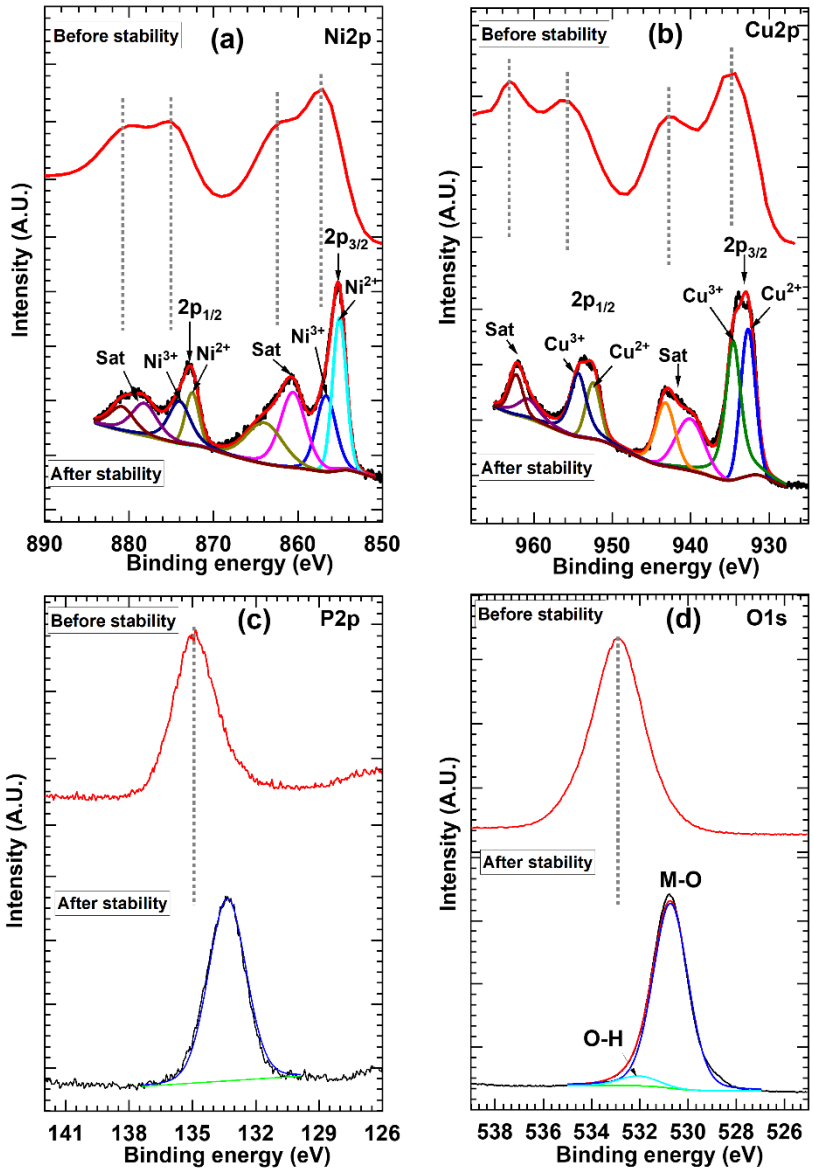


**S8:** XPS spectra of (i) Ni2p, (ii) Cu2p, (iii) P2p, and (iv) O1s for nickel copper phosphate (NCP-S3) samples before and after stability test.

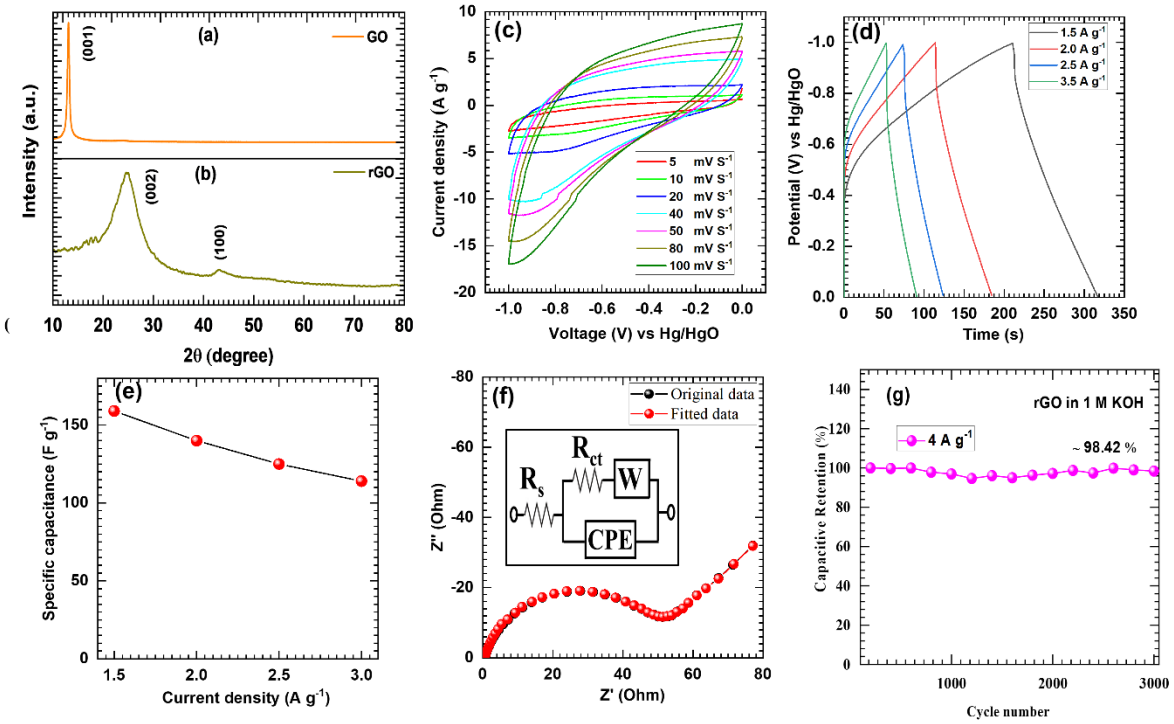


**S9:** (a) XRD patterns of (a) GO and (b) rGO samples, (c) CV plots of rGO electrode at scan rates from 5-100 mV $s^{-1}$, (d) the GCD curves of rGO electrode at different current densities from 1.5 to 3.5 A $g^{-1}$, (e) the plot of specific capacitance of rGO electrode at 1.5 to 3.5 A $g^{-1}$ current densities, (f) Nyquist plot of rGO electrode [Inset: equivalent circuit for fitted with Nyquist plot and (g) stability of rGO electrode during 3000 cycles at current density of 4 A $g^{-1}$.

Graphene oxide (GO) was prepared by modified Hummer's method, and further, it was reduced hydrothermally to prepare reduced graphene oxide (rGO). XRD patterns of GO and rGO are presented in Fig. S8 (a and b). The prepared GO sheet showed the strong characteristic peak at 11.13° assigned to the (0 0 1) plane in the XRD. Also, the characteristic diffraction peaks of rGO are detected at 24.71° and 43.09° assigned to the (0 0 2) and (1 0 0) planes [S1]. The scattered XRD peak at 24.71° confirms a reduction of GO material and formation of few layered rGO nanosheets [S2].

The electrochemical characteristics of rGO electrode tested by CV, GCD and EIS techniques in 1 M KOH electrolyte using three-electrode cell configuration. The CV curves of rGO (negative) electrode at various scan rates from 5-100 mV $s^{-1}$ within the potential range of 0 to -1 V vs Hg/HgO in 1 M KOH electrolyte are displayed in Figure S8 (c). Fig. S8 (c) shows that, the area under the CV curve increases with increasing scan rate, this displays voltammetric current is proportional to the scan rate of CV and signifies typical EDLC behaviour of electrode. The quasi-rectangular profile of CV curves affirms EDLC based capacitive nature of rGO electrode.

The GCD plots of rGO electrode evaluated at different current densities from 1.5 to 3.5 A $g^{-1}$ within the potential range of 0 to -1 V vs Hg/HgO and presented in Fig. S8 (d). The charge-discharge plot shows nearly linear curve, which is the indicative of its double layer capacitive nature. The GCD analysis was used to calculate specific capacitance of rGO electrode and plotted in Fig. S8 (e) as a function of current density. The maximum specific capacitance of 159 F $g^{-1}$ is obtained for rGO electrode at 1.5 A $g^{-1}$ current density and it decreases to 114 F $g^{-1}$ at the current density of 3.5 A $g^{-1}$.

The EIS study of rGO electrode was executed to examine its electrochemical conductivity. The Nyquist plot of rGO electrode is exhibited in Fig. S9 (f). The fitted equivalent circuit is displayed as inset of Fig. S8 (f). In fitted circuit, $R_s$ =0.48 Ω, $R_{ct}$ =47.61 Ω, CPE =0.843 mF and W =0.282 Ω. A small value ($R_s$ and $R_{ct}$) of total impedance denotes excellent electrical conductivity of rGO electrode. The cyclic stability of the rGO electrode was tested over 3000 GCD cycles at a current density of 4 A $g^{-1}$ and presented in Fig. S9 (g). This stability test revealed 98.42% retention of the specific capacitance after 3000 GCD cycles. Such an excellent cyclic stability of cathode and anode is owing to the amorphous nature (Nickel copper phosphate) and EDLC charge storage mechanism (rGO) of electrode

materials, respectively. The capacitive performance of rGO in negative potential window suggests its application as anode in hybrid device.

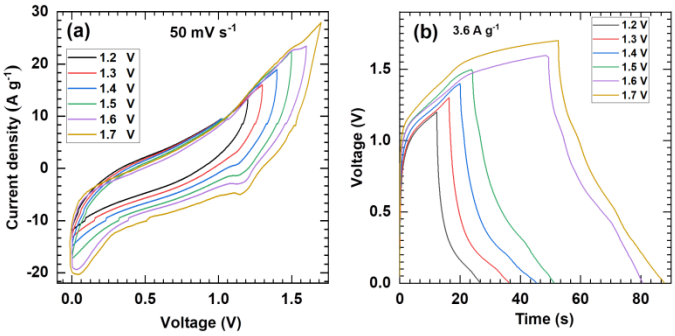


**S10:** (a) CV plots of HAASC device in different voltage windows from +1.2 to +1.7 V at fixed scan rate 20 mV $s^{-1}$, (b) GCD curves of HAASC device in different voltage windows at +1.2 to +1.7 V at fixed current density 1.7 A $g^{-1}$.

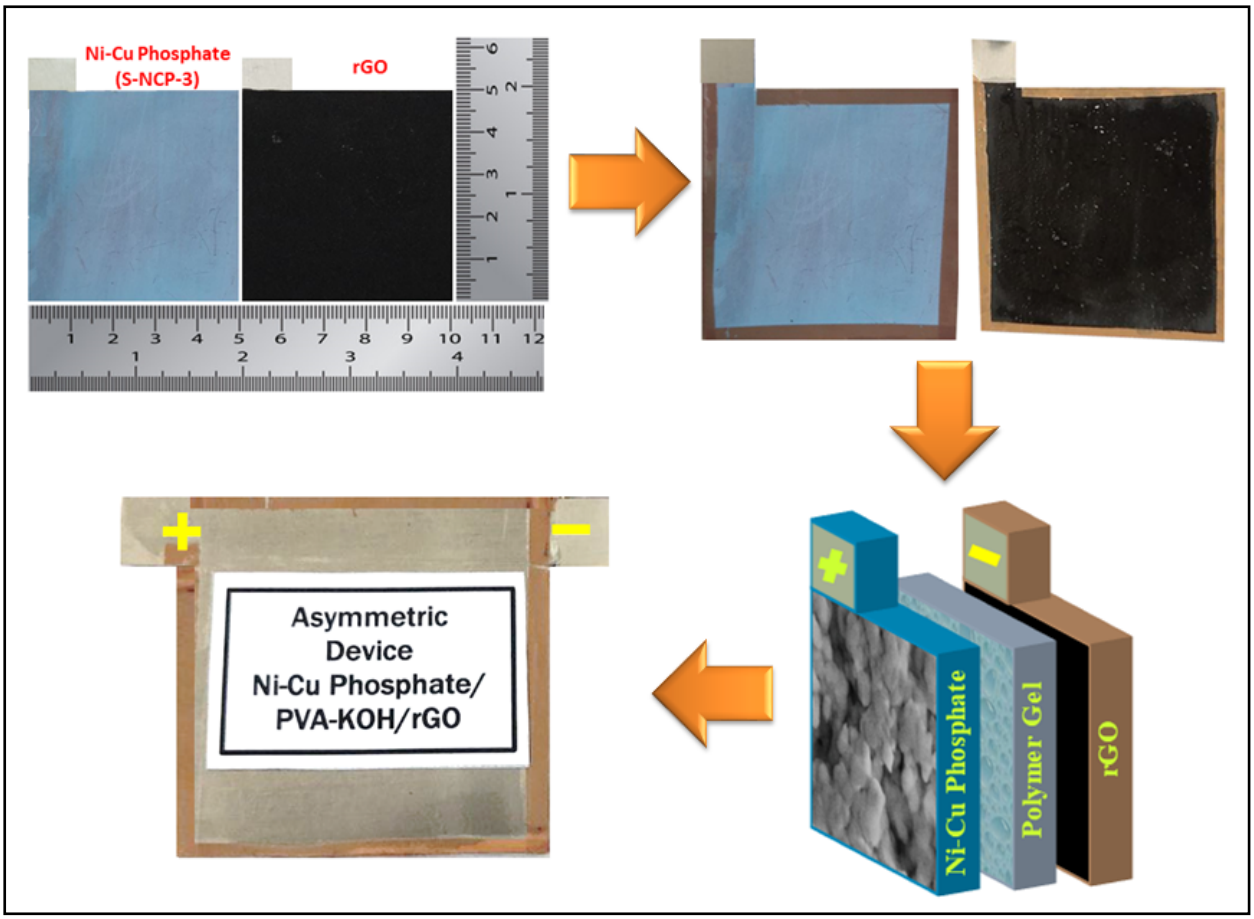


**S11:** Schematic illustration of HASASC device fabrication.

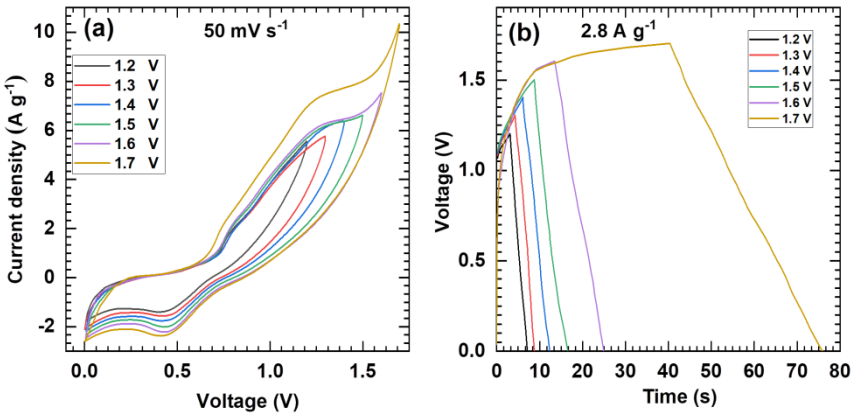


**S12:** (a) CV plots of HASASC device in different voltage windows from +1.2 to +1.7 V at fixed scan rate 20 mV $s^{-1}$, (b) GCD curves of HASASC device in different voltage windows at +1.2 to +1.7 V at fixed current density 2.0 A $g^{-1}$.

**Table S1:** Different compositions of nickel and copper precursors for the synthesis of amorphous nickel copper phosphate thin films and the corresponding notations**.**

| Sr. No. | $NiSO_4.6H_2O$ (M) | $CuSO_4.5H_2O$ (M) | $K_2HPO_4$ (M) | Notation |
|---|---|---|---|---|
| 1. | 0.033 | 0.000 | 0.075 | NCP-S1 |
| 2. | 0.0083 | 0.0249 | 0.075 | NCP-S2 |
| 3. | 0.0166 | 0.0166 | 0.075 | NCP-S3 |
| 4. | 0.0249 | 0.0083 | 0.075 | NCP-S4 |
| 5. | 0.000 | 0.033 | 0.075 | NCP-S5 |

**Table S2:** Experimental and observed nickel and copper atomic ratio in NCP-S series thin films.

| Sample name | Experimental ratio (Ni:Cu) | Observed ratio (Ni:Cu) | Obtained phase |
|---|---|---|---|
| NCP-S1 | 1:0 | 1:0 | $Ni_3(PO_4)_2 \cdot nH_2O$ |
| NCP-S2 | 0.75:0.25 | 0.70:0.30 | $Ni_{2.10}Cu_{0.90}(PO_4)_2 \cdot nH_2O$ |
| NCP-S3 | 0.50:0.50 | 0.52:0.48 | $Ni_{1.56}Cu_{1.44}(PO_4)_2 \cdot nH_2O$ |
| NCP-S4 | 0.25:0.75 | 0.20:0.80 | $Ni_{0.60}Cu_{2.40}(PO_4)_2 \cdot nH_2O$ |
| NCP-S5 | 0:1 | 0:1 | $Cu_3(PO_4)_2 \cdot nH_2O$ |

**Table S3**: Electrochemical performance comparison of various amorphous nickel copper phosphate/pyrophosphate based electrodes.

| Sr. No. | Material | Substrate | Method of deposition | Electrolyte | Capacitance (F $g^{-1}$) at current density (A $g^{-1}$) | Ref. |
|---|---|---|---|---|---|---|
| 1 | $Cu_2P_2O_7$ | Stainless steel | SILAR | 1 M LiCl | 332.9 F $g^{-1}$ at 10 A $g^{-1}$ | 31 |
| 2 | $Cu_2P_2O_7$ | Stainless steel | SILAR | 1.5 M LiCl | 465 F $g^{-1}$ at | 32 |
| 3. | $Cu_2P_2O_7$ | Nickel foam | Hydrothermal with subsequent calcination | 3 M KOH | 297.521 F $g^{-1}$ at 1 A $g^{-1}$ | S3 |
| 4 | $Cu_2(PO_4)OH$ | Stainless steel | Hydrothermal | 1 M KOH | 137.02 F $g^{-1}$ at 0.4 mA $cm^{-2}$ | S4 |
| 5 | $Cu_3P$ NT | Copper foil | electro-oxidation | 1 M $H_2SO_4$ | 300.9 at 2.5 mA $cm^{-2}$ | S5 |
| 6. | $Cu_{3(}PO_4)_2$ | Nickel foam | Solvothermal | 2 M KOH | 309.75 F $g^{-1}$ at 0.5 A $g^{-1}$ | S6 |
| 7 | $Ni_3(PO_4)_2$ | Nickel foam | Sonochemical | 1 M KOH | 620 C $g^{-1}$ at 0.4 A $g^{-1}$ | S7 |
| 8 | $Ni_2P_2O_7$ | Nickel foam | hydrothermal | 3 M NaOH | 557.7 F $g^{-1}$ at 1.2 A $g^{-1}$ | S8 |
| 9 | $(Ni_{11}(HPO_3)8(OH)_6$ | Nickel foam | hydrothermal | 3 M KOH | 295 F $g^{-1}$ at 0.625 A $g^{-1}$ | S9 |
| 10 | Nickel Pyrophosphate | Nickel foam | hydrothermal | 1 M KOH | 224 F $g^{-1}$ at 1 A $g^{-1}$ | S10 |
| 11 | $Ni_{11}(HPO_3)_8(OH)_6$ | Nickel foam | hydrothermal | 3 M KOH | 558 F $g^{-1}$ at 0.5 A $g^{-1}$ | S11 |
| 12 | **Nickel copper phosphate** | **Stainless steel** | **hydrothermal** | **1 M KOH** | **711 F $g^{-1}$ at 1 A $g^{-1}$** | **Present work** |

**Table S4:** Electrochemical impedance spectroscopic fitted circuit parameters of NCP-S series.

| Sample name | $R_s$ (Ω) | $R_{ct}$ (Ω) | CPE (mF) | n | W (Ω) |
|---|---|---|---|---|---|
| **NCP-S1** | 0.55 | 0.70 | 0.81 | 0.98 | 0.61 |
| **NCP-S2** | 0.45 | 1.04 | 1.19 | 0.88 | 0.82 |
| **NCP-S3** | 0.33 | 0.38 | 0.90 | 0.93 | 0.90 |
| **NCP-S4** | 0.48 | 0.87 | 0.61 | 1.0 | 0.16 |
| **NCP-S5** | 0.38 | 1.20 | 1.53 | 0.82 | 0.44 |

**Table S5:** The comparative electrochemical performance for HAASC and HASASC devices is compared with previous metal phosphate based devices.

| Sr. No. | Positive electrode | Negative electrode | Electrolyte | Specific energy (Wh $kg^{-1}$) | Specific power (kW $kg^{-1}$) | Stability at cycles | Ref. |
|---|---|---|---|---|---|---|---|
| 1. | $Ni_{0.75}Mn_{0.25}(PO_4)_2$/NF | activated carbon | 1 M KOH | 63.8 | 11.89 | 99.2% 5000 | 18 |
| 2. | $Ni_{1.38}Co_{1.62}(PO_4)_2 \cdot 8H_2O$ | rGO/SS | 1 M KOH | 36.02 | 0.16 | 83.7% 4000 | 19 |
| 2. | Ni-Cu-P/NF | activated carbon | 2 M KOH | 40.5 | 0.87 | 98.5% 10000 | 24 |
| 3. | FeCoCuP/NF | activated carbon | 2 M KOH | 61.5 | 0.12 | 88.7% 5000 | 58 |
| 4. | $NaNi_4(PO_4)_3$/GF | activated carbon | 2 M $NaNO_3$ | 19.5 | 0.57 | 94% 5000 | 59 |
| 5. | Ni-CoP@C@CNT | Graphene | 3 M KOH | 17.4 | 0.69 | 117% 5000 | 60 |
| 6. | Ni-P@$NiCo_2O_4$ | activated carbon | 6 M KOH | 13.3 | 5.7 | 78.3% 10000 | 61 |
| 7. | $NaNiPO_4$ | activated carbon | 1 M NaOH | 20 | 0.13 | 95% 500 | 62 |
| 8. | $NaNi_{0.33}Co_{0.67}PO_4.H_2O$/NF | Graphene | 1 M KOH | 29.85 | 0.37 | 76.9% 10000 | 63 |
| 9. | T-$Nb_2O_5$@$Ni_2P$/NF | activated carbon | 3 M KOH | 30.2 | 0.45 | 92% 5000 | 64 |
| 10. | NiCoP@NF | activated carbon | 6 M KOH | 27 | 0.64 | 67.2% 500 | 65 |
| **11.** | **$Ni_{1.56}Cu_{1.44}(PO_4)_2 \cdot H_2O$/SS** | **rGO/SS** | **1 M KOH** | **34** | **2.40** | **94.11 % 5000** | **Present work** |
| | | | **PVA-KOH** | **13.51** | **0.55** | **93.81% 5000** | |

**References:**


31. A. Agarwal and B. Sankapal, *Chem. Eng. J*. 2021, **422**, 130131.

32. A. Agarwal, S. Majumder and B. Sankapal, *Int. J. Energy Res.*, 2021, **46**, 6177-6196.

S1. M. Mohamed and D. Bhat, *AIMS Mater Sci*, 2017, **4**, 158-171.

S2. B. Ahmed, A. Ojha, F. Hirsch, I. Fischer, D. Patrice and A. Materny, *RSC Adv.*, **7**, 2017, 13985-13996.

S3 A. Karaphun, P. Chirawatkul, S. Maensiri and E. Swatsitang, *J. Sol-Gel Sci. Technol.*, **88**, 2018, 407-421.

S4 S. Pujari, S. Kadam, Y-R. Ma, P. Katkar, S. Marje, S. Khalate, A. Lokhande and U. Patil, *J. Electron Mater.*, 2020, **49**, 3890-3901.

S5 Y-C. Chen, Z-B. Chen, Y-G. Lin, Y-K. Hsu, *ACS Sustainable Chem. Eng.*, 2017, **5**, 3863-3870.

S6 B. Saravanakumar, A. Haritha, G. Ravi and R. Yuvakkumar, *J. Nanosci. Nanotechnol*, 2020, **20**, 2813-2822.

S7 F. Omar, A. Numan, N. Duraisamy, S. Bashir, K. Ramesh, S. Ramesh, *RSC Adv.*, 2016, **6**, 76298-76306.

S8 C. Wei, C. Cheng, S. Wang, Y. Xu, J. Wang and H. Pang, *Chem. Asian J.*, 2015, **10**, 1731-1737.

S9 H. Pang, Z. Yan, Y. Wei, X. Li, J. Li, L. Zhang, J. Chen, J. Zhang and H. Zheng, *Part. Part. Syst. Charact,* 2013, **30**, 287-295.

S10 K. Sankar, Y. Seo, S. Lee and S. Jun, *ACS Appl. Mater. Interfaces*, 2018, **10**, 8045-8056.

S11 Y. Gao, J. Zhao, Z. Run, G. Zhang and H. Pang, *Dalton Trans.*, 2014, **43**, 17000-17005.